PNAS RESEARCH ARTICLE | PHYSICS

Quantum Barkhausen noise induced by domain wall cotunneling

C. Simon[a], D.M. Silevitch[a], P.C.E. Stamp[a,b,c,1], and T.F. Rosenbaum[a,1]

Edited by J.C. Davis, University of Oxford, Oxford, United Kingdom; received September 7, 2023; accepted February 14, 2024

Most macroscopic magnetic phenomena (including magnetic hysteresis) are typically understood classically. Here, we examine the dynamics of a uniaxial rare-earth ferromagnet deep within the quantum regime, so that domain wall motion, and the associated hysteresis, is initiated by quantum nucleation, which then grows into large-scale domain wall motion, which is observable as an unusual form of Barkhausen noise. We observe noncritical behavior in the resulting avalanche dynamics that only can be explained by going beyond traditional renormalization group methods or classical domain wall models. We find that this "quantum Barkhausen noise" exhibits two distinct mechanisms for domain wall movement, each of which is quantum-mechanical, but with very different dependences on an external magnetic field applied transverse to the spin (Ising) axis. These observations can be understood in terms of the correlated motion of pairs of domain walls, nucleated by cotunneling of plaquettes (sections of domain wall), with plaquette pairs correlated by dipolar interactions; this correlation is suppressed by the transverse field. Similar macroscopic correlations may be expected to appear in the hysteresis of other systems with long-range interactions.

magnetic noise | quantum nucleation | quantum Ising

Significance

Noise phenomena are ubiquitous in nature and often are regarded as an unfortunate background that confounds desirable signals. However, the distribution and correlations of the noise itself can reveal much of the underlying physics of a material. Here, we find that, in our carefully chosen system, the "Barkhausen noise" present in all magnets is actually dominated by correlated quantum tunneling phenomena, in which millions of billions of spins tunnel together to produce "quantum noise." Understanding how such large-scale quantum effects can be created and controlled is an essential element for developing new devices and applications that depend on quantum coherence, such as qubit processors.

Although magnetism at the microscopic scale has been understood as a quantum phenomenon for nearly a century, macroscopic magnetic objects like domain walls are usually treated classically (1–7). There is good reason for this: In a conductor, the dissipative coupling to electrons rapidly suppresses domain wall tunneling (8, 9), and even in an insulator, the coupling to phonons (10, 11), paramagnetic impurities (11), and nuclear spins (11) is enough to render the wall motion classical, except at microscopic scales. These mechanisms also suppress "chiral tunneling" (11–13) between opposite chiralities for a given wall; for a Bloch wall, the chirality is simply the sense (clockwise or anticlockwise) in which the magnetization winds in passing between the states on either side of the wall.

It is actually very difficult to observe the dynamics of individual domain walls except in restricted geometries. More typically, one sees evidence of collective "multi-wall" motion, either by imaging walls before and after this motion has occurred, or by measurements of the dynamic susceptibility $\chi(\omega)$, or of the "Barkhausen noise" in the bulk magnet. The latter shows up in inductive measurements, arising from rapid jumps in the magnetization caused by the depinning of walls and their subsequent motion. Since the discovery of Barkhausen noise in 1919 (14), a vast corpus of experimental work has accumulated, characterizing the influence on the noise of disorder, different magnetic interactions, and the proximity to phase transitions (15–19). However, all of this work has been done on thermally activated wall motion—there have been no investigations of quantum Barkhausen noise, in which domain wall tunneling, rather than thermal excitation over barriers, dominates.

The present study explores this quantum regime. Just as in the classical regime, we expect interwall interactions, mediated by dipolar interactions, to lead to collective wall dynamics and even avalanche processes under the right conditions. We also expect the coupling to phonons to play a role.

To disentangle the different processes, it is important to choose the right experimental system. We need the wall structure to be simple, and to see quantum behavior, we need the crossover between classical thermal activation and quantum tunneling to be at sufficiently high temperature. An ideal system is the Ising magnet $LiHo_xY_{1-x}F_4$, in which very strong crystal fields acting on the $J = 8$ Ho electronic spins create a low-temperature Ising doublet with renormalized moment $\tilde{J} \approx 5.51\mu_B$, separated from the 1st excited state by a gap $\Delta \approx 9.4$ K.

When $T \ll \Delta$, the system can be described by an effective Hamiltonian $\mathcal{H} = \mathcal{H}_{QI} + \mathcal{H}_{env}$, where $\mathcal{H}_{QI}$ is the quantum Ising Hamiltonian:

Author affiliations: [a]Division of Physics, Mathematics, and Astronomy, California Institute of Technology, Pasadena, CA 91125; [b]Department of Physics and Astronomy, University of British Columbia, Vancouver, BC V6T 1Z1, Canada; and [c]Pacific Institute of Theoretical Physics, University of British Columbia, Vancouver, BC V6T 1Z1, Canada

Author contributions: C.S., D.M.S., P.C.E.S., and T.F.R. designed research; C.S. and D.M.S. performed research; C.S., D.M.S., P.C.E.S., and T.F.R. analyzed data; and C.S., D.M.S., P.C.E.S., and T.F.R. wrote the paper.

The authors declare no competing interest.

This article is a PNAS Direct Submission.

[1]To whom correspondence may be addressed. Email: stamp@phas.ubc.ca or tfr@caltech.edu.

This article contains supporting information online at https://www.pnas.org/lookup/suppl/doi:10.1073/pnas.2315598121/-/DCSupplemental.

Published March 19, 2024.

$$\mathcal{H}_{\mathrm{QI}} = -\sum_{i \neq j} V_{ij}^{zz} \sigma_i^z \sigma_j^z - \Gamma_0(B_x) \sum_i \sigma_i^x, \qquad [1]$$

with a longitudinal dipolar interaction V_{ij}^{zz} and a bare splitting $\Gamma_0(B_x)$ induced in the Ising doublet by a transverse field B_x. The "environmental" term $\mathcal{H}_{\mathrm{env}}$ has the form

$$\mathcal{H}_{\mathrm{env}} = \mathcal{H}_{\mathrm{hyp}} + \mathcal{H}_{\mathrm{ph}} + \mathcal{H}_{\mathrm{EM}} + \mathcal{H}_{\mathrm{disorder}}, \qquad [2]$$

where the first three terms refer to hyperfine interactions, spin-phonon interactions, and interactions with the electromagnetic field, and the final term describes the effect of disorder when the concentration of Holmium $x < 1$. For details of this Hamiltonian and its derivation, see *SI Appendix*, section 1.

The main effect of $\mathcal{H}_{\mathrm{hyp}}$ is to block flips between the $|\uparrow\rangle$ and $|\downarrow\rangle$ states of the Ising doublet (20, 21) until $B_x \sim 2$ T, giving a much reduced effective splitting $\tilde{\Gamma}(B_x)$. The spin-phonon terms facilitate irreversible phonon-assisted flips, and $\mathcal{H}_{\mathrm{EM}}$ contains the demagnetization field generated by the spins, which depends on sample shape. Finally, when $x < 1$, off-diagonal dipolar terms $\sim V_{ij}^{zx}\sigma_i^z\sigma_j^x$ are generated (20–22), so that an applied longitudinal field generates a random transverse field, and an applied transverse field generates a random longitudinal field.

Very thin domain walls (with thickness $\lambda < a_0$, the lattice spacing) are allowed because the exchange interaction between spins is negligible. The easy axis $\hat{z}$ lies in the wall plane and the wall orientation is controlled by pinning forces and the demagnetization fields. As noted many years ago by Egami (23, 24), domain wall motion for such walls involves the nucleation and growth of "plaquette" distortions of the wall, in which a small section of the wall shifts locally by a single lattice spacing. In the presence of an external field along the easy z-axis, the plaquette can tunnel through a barrier created by the energy associated with the wall distortion, and then grow once it exceeds a critical size. This nucleation also requires a local transverse field to flip individual spins (otherwise $[\mathcal{H}, \sigma_i^z] = 0$). Such a field can be applied come from transverse demagnetization, or arise from the disorder-induced terms $\sim\sigma_i^z\sigma_j^x$ noted above.

Domain walls previously have been imaged in the $LiHo_xY_{1-x}F_4$ system (25, 26), and indirect evidence for tunneling motion has been found in low-temperature susceptibility measurements in transverse magnetic field (5–7). A priori we expect the crossover between thermal activation and tunneling to occur at a relatively high temperature compared to typical Bloch wall systems because the wall is so thin, because very small regions are involved in plaquette formation, and because the characteristic frequency of spin flips is high. Taken together, these characteristics make the $LiHo_xY_{1-x}F_4$ system a good candidate for low-temperature tunneling behavior.

1. Results

In the experiments described here, we made both quasistatic bulk magnetization measurements and faster time-domain measurements of individual magnetic avalanches known as "Barkhausen events" (14) on a single crystal of $LiHo_{0.4}Y_{0.6}F_4$ at temperatures ranging from 15% (90 mK) to 95% (580 mK) of the Curie temperature, $T_C = 612$ mK, as the external longitudinal field (along the Ising axis) was ramped between $H_\parallel = \pm 4$ kOe—a field sufficiently large to saturate the magnetization. Additionally, a static external field transverse to the Ising axis was applied at several values ranging from $H_\perp = 0 \rightarrow 200$ Oe. We emphasize that we measure quantum Barkhausen noise. A diagram of the experimental setup is shown in Fig. 1.

When comparing the DC bulk magnetization of the sample at different temperatures (Fig. 2*A*), it is apparent that, at a macroscopic level, the effect of increasing temperature is to decrease the saturation magnetization, affecting the outer portions of the hysteresis loop at fields $|H_\parallel| > 1$ kOe, but leaving the "linear" regime of the hysteresis loop unchanged at lower fields $|H_\parallel| < 1$ kOe. Furthermore, the strength of the transverse fields applied in these measurements ($H_\perp \leq 200$ Oe) was sufficiently weak that they had no observable effect on any portion of the hysteresis loop.

In many soft ferromagnets, the creation/annihilation of individual domains is found to occur at external longitudinal fields close to saturation (27), while the linear regime at lower fields is dominated by the motion of domain walls. Since we are primarily interested in the dynamics of the motion of domain walls, we restrict our analysis to this linear regime at low fields ($|H_\parallel| < 600$ Oe).

Even from 15% to 95% of T_C, there is no change in the sample response (Fig. 2*A*), indicating that thermal fluctuations are unimportant in the dynamics of the domain wall motion. This implies that for all temperatures and fields, the domain wall dynamics are driven by quantum, rather than thermal, fluctuations. This is to be contrasted with a previous measurement (6) on a sample of similar Ho concentration $x = 0.44$ (as opposed to our $x = 0.4$), in which, under no transverse field, the hysteresis loop narrowed considerably from low (100 mK) to high (500 mK) temperature. The essential difference between these two measurements is the sample shape. In the present measurements, a cuboid with an aspect ratio $1\times1\times2$ was used, as opposed to the measurements in ref. 6 performed on a needle with a much longer aspect ratio.

Since neither sample is an ellipsoid, the demagnetization field will not be spatially homogeneous. Moreover, it will introduce transverse demagnetization fields in addition to the longitudinal components. The shorter aspect ratio of the cuboid not only decreases the average longitudinal internal field in comparison to the needle, but it will also broaden the distribution of both the longitudinal and transverse fields. We have calculated

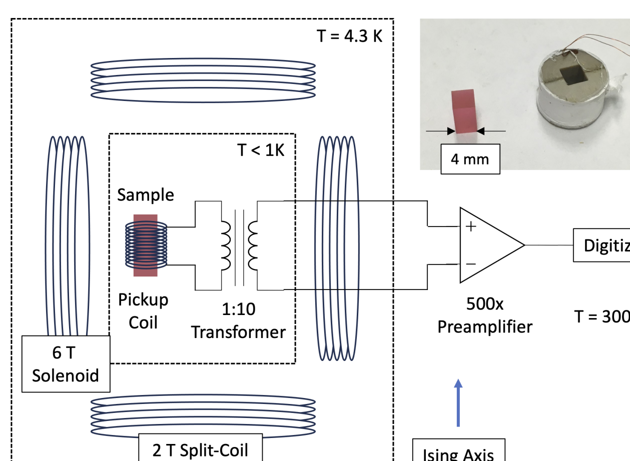

Fig. 1. Schematic of experimental setup. An inductive pickup coil is wound around the crystal of $LiHo_{0.40}Y_{0.60}F_4$ inside an insulating PEEK coil form. The assembly is mounted on the Cu cold finger of a helium dilution refrigerator equipped with a 6T/2T superconducting vector magnet. The induced voltage signal is amplified first by a cryogenic broadband transformer amplifier, and then at room temperature by a low-noise transistor preamplifier and finally digitized with a streaming oscilloscope. *Inset*: Photograph of sample and pickup coil assembly.

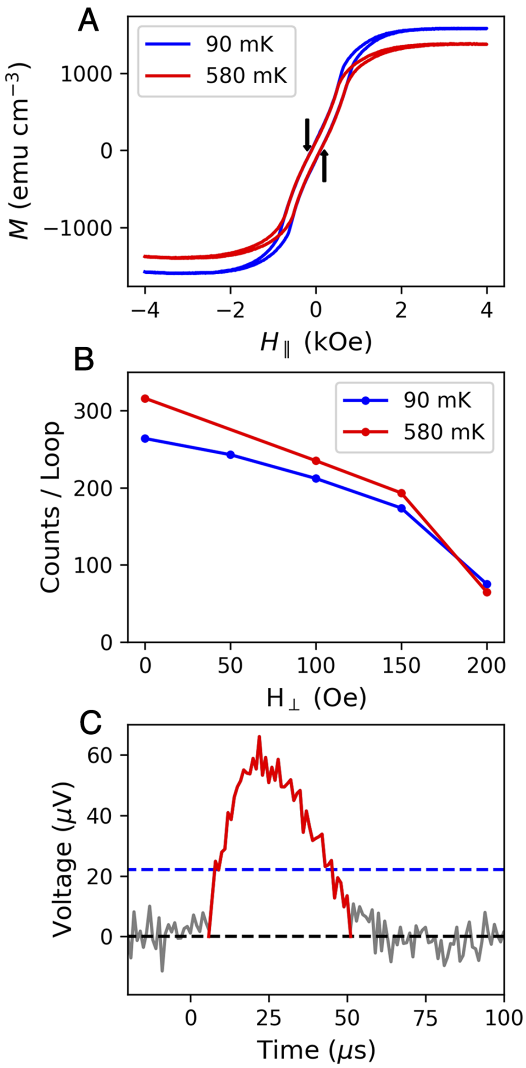

Fig. 2. Hysteresis loops and Barkhausen events for extremal temperatures. (*A*) Magnetization vs. longitudinal field curves at temperatures 15% and 95% of the Curie temperature with $H_\perp = 0$.Loops at transverse fields up to 200 Oe are indistinguishable from those at zero transverse field. (*B*) Average number of detected events per loop for a given temperature and transverse field. (*C*) Event extraction for a sample event. Data in gray are the raw extracted voltages, blue is the detection threshold, and red is the extracted event.

numerically the demagnetization fields resulting from a homogeneous bulk magnetization of ∼100 Oe along the Ising axis, corresponding to the sample magnetization measured by the Hall magnetometer at an external longitudinal field of ∼200 Oe, where most of the Barkhausen events occur (see *SI Appendix*, section 4 for details). These calculations show that the cuboid has a longitudinal field width approximately 20× that of the needle (∼10 G vs. ∼0.5 G), and a transverse field width approximately 50× larger than that of the needle (∼5 G vs. ∼0.1 G).

The effect of the longitudinal field distribution on the domain dynamics is to introduce a variance in the pinning energy given by $\mu_{\mathrm{Ising}} h_\parallel$ where μ_{Ising} is the magnitude of the Ising moment of a single spin, and $h_\parallel$ is the strength of the longitudinal field. This results in a distribution of pinning energies due to a shape-dependent demagnetization of ∼4.6 mK for the cuboid and ∼0.23 mK for the needle geometry.

The transverse field has a much more complicated effect. For a single ion, an external transverse field both lowers the energy of the spin (independent of its instantaneous electronic state) and generates quantum fluctuations. Since we are considering the coupled dynamics of many spins, we must also take into consideration the off-diagonal dipolar interaction V_{ij}^{zx}, which scales as the local transverse field. This interaction generates two main terms: one $\sim\sigma_i^z\sigma_j^x$ that induces quantum fluctuations, and another $\sim\sigma_i^z\sigma_j^0$ (with σ_j^0 as the identity matrix) that classically suppresses ordering through an effective three-spin interaction (28).

We conclude that the increased quantum fluctuations in our cuboid sample (in comparison to the needle geometry), arising from the shape-dependent transverse fields, drive up the crossover temperature from quantum to classical behavior, thereby keeping our sample deep in the quantum regime even at temperatures approaching the classical phase transition.

While the application of a modest external transverse field ($H_\perp = 200$ Oe) has no observable impacts on the macroscopic sample response at slower timescales (∼1 s), the situation changes dramatically when analyzing individual avalanches on a μs timescale. The motion of individual domains on this timescale was measured by digitizing the voltage output of an inductive pickup coil measuring the time-derivative of the sample magnetization, $\mathrm{d}M/\mathrm{d}t$, recorded on an oscilloscope sampling at 1 MHz. Using a thresholding technique as shown in Fig. 2*C* (see *Materials and Methods* for details), individual avalanches with voltages rising above the noise floor were extracted in software, and the statistics of their metrics (duration T and area S among others) were analyzed, along with cross-correlations between the various metrics according to traditional crackling noise analysis (29, 30). The full set of detected Barkhausen events are available at the CaltechDATA repository (31).

We note that the only events that we are able to observe correspond to the largest avalanches. The detectable avalanches range in size from $\approx 2 \times 10^{-10}$ Wb $\rightarrow 6 \times 10^{-9}$ Wb, corresponding to avalanches containing a number of spins N between 1.5×10^{15} and 4.5×10^{16} spins. The change in the macroscopic magnetization over the full hysteresis loop (Fig. 2*A*) is actually dominated by the multiplicity of smaller domain flips below our noise floor, with the change in magnetization due to the measured large events contributing anywhere from ∼0.01% (at $H_\perp = 0$) to ∼0.1% (at $H_\perp = 200$ Oe) of the total change in magnetization of the entire sample over the full loop. All events were observed in a narrow region between 150 Oe $\leq H_\parallel \leq$ 200 Oe while ramping up, and at the equivalent negative field while ramping down (marked by arrows in Fig. 2*A*). By contrast to previous susceptibility measurements (5) that measured only the domain walls with weakest pinning, in this experiment we measure only the most strongly pinned domain walls. The larger pinning potential requires a larger external drive field to depin the domain wall, leading to larger magnetization reversals before long-range dipolar forces can pin the domain wall in place. The end result is larger avalanches.

While traditional Barkhausen analysis consists of deducing the underlying universality class by extracting the critical exponents through power-law fits of event statistics (29, 30), or by using lineshape analysis to learn about underlying dissipative or demagnetization effects (7, 32–34), this is not appropriate here because our data does not display the standard power-laws characteristic of universality. Instead, we observe two distinct classes of events, presumably corresponding to two different domain-wall activation mechanisms, that show remarkably different dependences on applied transverse fields.

The noncritical behavior is most easily observed by comparing the two-dimensional histograms plotting the cross-correlation between event duration (T) and area ($S = \int_0^T V\,\mathrm{d}t$) for the most extreme temperatures (90 and 580 mK) and transverse fields (0 and 200 Oe). As seen in Fig. 3*A*, the events separate into two distinguishable classes at low fields. The first class, which we label as "independent" (indicated by the orange arrow in Fig. 3*A*), approximately follows a power-law with an exponent of $\approx$1.1 [close to the power of 1 indicative of avalanches (33)] over approximately one decade of duration. The second class, which we designate "cooperative" (indicated by the red arrow in Fig. 3*A*) that appears as an approximately Gaussian cluster over a more limited range of durations with higher areas for any given duration than events in the independent class. Furthermore, while the frequency of the independent events decreases only modestly with transverse field, the cooperative events are suppressed almost completely with a 200 Oe transverse field. We have plotted one sample event in each class in Fig. 3*B*, both marked by arrows on the 2d histograms in Fig. 3*A*, with the cooperative event in red and the independent event in orange.

2. Discussion

In the following discussion, we discuss the possible origins of these two activation mechanisms, as well as phenomenologically explain why such a small 200 Oe transverse field could suppress the cooperative events starting from the microscopic Hamiltonian.

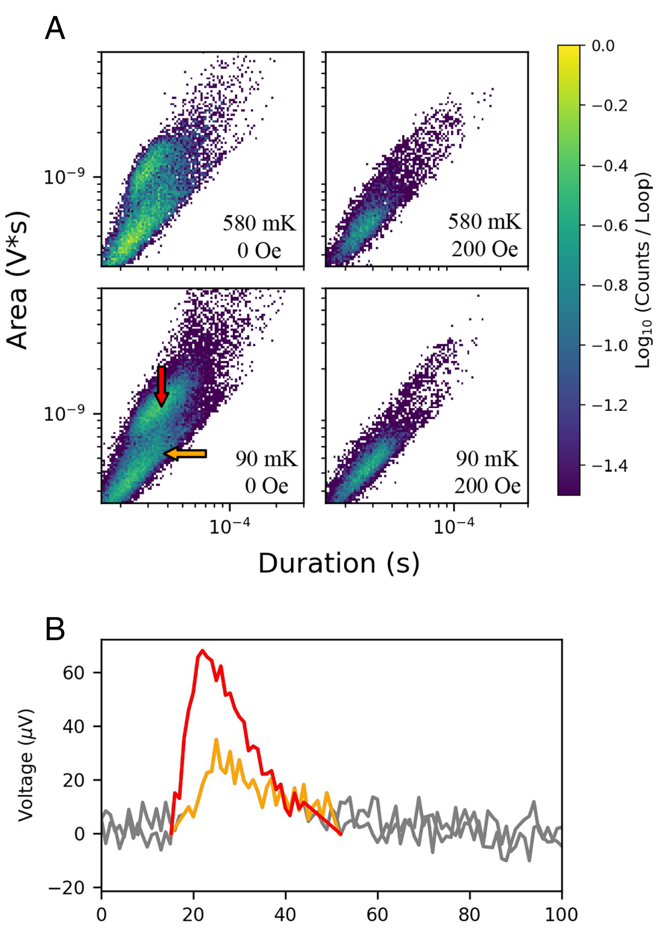

Fig. 3. Classes of events. (*A*) 2D histograms of event area vs. event duration for low/high temperatures and zero/non-zero transverse fields. (*B*) Sample events of each class: independent event in orange, and cooperative event in red as indicated by the colored arrows in (*A*).

First, we deduce that both activation mechanisms are quantum mechanical in nature. Like the magnetization curves within the linear regime, the event statistics show the same temperature independence, demonstrating that within this experimental parameter range, the sample is deep within the quantum regime. The initial nucleation is governed by quantum tunneling, rather than thermal activation, of spins.

While the resulting avalanche will release energy and locally heat the surrounding spins, the temperature increase is not sufficient to cause a small thermal runaway. The local temperature rise can be estimated by $E = H \cdot \delta M = C_V \delta T$, where the energy of a spin flip is given by the local field ($\sim$200 G) multiplied by the change in magnetization ($2 \times \mu_{\mathrm{Ising}} \sim 14\mu_B$, where μ_{Ising} is the single spin moment and μ_B is the Bohr magneton). Using the specific heat $C_V/R \sim 1$ from ref. 35 in these temperature ranges gives a local temperature rise of approximately 200 mK. The only way for a thermal runaway to occur at the temperature of the experiments (90 mK) is if the heat generated by the avalanches is sufficient to heat the system well above the highest temperature (580 mK), where we observe T-independent behavior. This is clearly not the case; the heat generated can only heat the system to roughly 300 mK, so we conclude that thermal runaway can be ruled out.

Given that both activation mechanisms are due to quantum tunneling (rather than one being quantum and the other thermal), one must figure out how there could be two different quantum tunneling mechanisms, why these two tunneling mechanisms have such dramatically different transverse field dependence, and how such a small 200 Oe field could suppress markedly either class of events.

Given this challenge, it is necessary to go beyond the theoretical picture of single independent wall tunneling and consider the interaction between walls. In so doing, we recover a phenomenological model in which the two different activation mechanisms correspond, on the one hand, to walls tunneling independently of each other and, on the other, to cooperative tunneling of pairs of walls. Cotunneling of domain walls is strongly affected by the application of an external transverse field much smaller than the fields required to induce single-spin tunneling.

First, we argue that there is only one type of domain wall that is supported by this material, even in the disordered case. For a system with very strong Ising anisotropy and very weak exchange interactions, the location of the domain wall between up and down domains is defined by the locus of points—the surface—on which the total local longitudinal field is zero (so that the field is entirely transverse). In this case, quantum or thermal fluctuations are seen in the existence of up spins on the down side of this surface and vice versa.

It has been understood for a long time that, for a strongly Ising system, the way in which the nucleation of domain wall motion must occur is via the nucleation of plaquettes (23, 24). The argument is simple—we only have the dipolar and anisotropy energies in the problem (if we ignore nuclear spins) and the lattice potential which acts on the domain wall position, as noted above (this is the point treated by Egami in refs. 23 and 24). Any other way of nucleating the domain wall motion would involve prohibitively high energies.

There are then well-defined contributions to the energy of a single plaquette: i) the "surface tension" associated with the plaquette periphery, which comes from a combination of the lattice potential and the dipolar interaction; and ii) the "bulk" energy, coming from the interaction of the magnetic field with the spins inside the plaquette. This is the picture introduced by Egami, and used since [e.g., by Mias and Girvin (36)]. In the case where we have $x = 1$, this is the standard picture. For $x = 0.4$ there will be an additional energy associated with pinning of the wall—but provided we can still consider walls in the sense defined above, this is the only new energetic contribution.

Under these circumstances, it is hard to see how one can have more than one kind of wall or more than one kind of wall motion nucleation process. Once the plaquette exceeds a critical size, it will start to grow rapidly and eventually become an avalanche, controlled by the bulk energy. This is in effect the standard "droplet nucleation" process.

We consider a model in which a single plane wall, or an adjacent pair of walls, can displace themselves through the system. A detailed consideration of this model is given in *SI Appendix*, sections 2 and 3, but we summarize the relevant conclusions of the theoretical treatment below.

To determine quantitatively from first principles the wall energetics is not easy, even when $x = 1$. This is because for a real system, we need to consider the spin dynamics of single spins, spin pairs, etc., in the presence of both spin-phonon and hyperfine interactions. To do this analytically is impossible, and it is also very difficult numerically because of the long-range dipolar interactions. Instead, we have adopted the time-honored method, going back to Landau-Lifshitz and Ginzburg–Landau, of writing an effective Hamiltonian which incorporates all the relevant energetics, and then writing our answers in terms of a set of effective couplings which must be determined from experiment. We emphasize that such an effective field theory approach has proved its usefulness, as for example in the case of superconductors—in our case, it allows us to identify the plaquette nucleation process as an essential element in the explanation for our experimental data, and it points to the importance of interplaquette interactions (see below).

Fortunately, we have a good idea of what the parameters in the theory can be. We start by noting that the energy required to flip a single Ising spin in the $LiHo_xY_{1-x}F_4$system is large compared to the temperature, since that process involves a transition via the first excited state at energy 9.4 K above the ground state. The energy associated with the periodic lattice potential acting on the wall must be of similar size and the small oscillation frequency associated with wall motion in this potential also will be of similar size.

It is well known that the crossover temperature between quantum tunneling and thermal activation for escape from a potential well is of the same order as the small oscillation frequency in the well. Thus, it is not surprising that we see tunneling up to the highest temperature in our experiments (580 mK).

It is also clear that the parameter describing the domain wall thickness must be less than the actual lattice spacing, at least for $x = 1$. For $x = 0.4$, it is not so clear, since we expect to find "satellite" spins away from the wall as defined by the surface discussed above. In the absence of further knowledge, we simply assume that this wall thickness is of the same order as the lattice spacing. We can in the same way argue that the wall pinning energy—which is the difference between the energy of the wall with and without a spin at the pinning site—will be of the same order as the Zeeman energy of that spin in the local field.

Even without disorder (for $x = 1$), the walls are pinned by a lattice periodic potential. Wall displacement then occurs by the nucleation of plaquettes of a displaced wall (Fig. 4*A*). This occurs by tunneling through a barrier created by the line tension in the plaquette periphery and the tunneling is driven by an applied longitudinal field. Plaquettes can nucleate at different parts of a wall, as well as on top of each other; they are the two-dimensional lattice version of quantum bubble nucleation (37).

When $x = 1$, the plaquette has energy

$$U_0[\vec{R}] = -g\mu_B \oint_R \mathrm{d}^2 r \vec{M}_p(\vec{r}) \cdot \vec{H}_0 + \frac{1}{2}\oint_{r_0} \mathrm{d}\vec{R} \int_{r_0} \mathrm{d}R' V_D(\vec{R} - \vec{R}'), \qquad [3]$$

where i) the two-dimensional integration is over the surface of the plaquette, and involves the magnetization density $\vec{M}_P(\vec{R})$ inside the plaquette volume; and ii) the one-dimensional integration is along the peripheral contour $\vec{R}$ of the plaquette, and involves the dipolar interaction $V_D(\vec{R} - \vec{R}')$ between the magnetic poles induced on this periphery. This dipolar interaction creates a "line tension" for the plaquette, which is minimized if the plaquette is circular; for such a circular plaquette, the energy $U_0(\vec{R}) \to U_0(R)$, where R is the plaquette radius, and we have

$$U_0(R) = -\pi g \mu_B \vec{\vec{J}} \cdot \vec{B}(R^2/a_0^2) + 2\pi\gamma_W R \ln(R/r_0), \qquad [4]$$

where we introduce the surface tension γ_W, and r_0 is the lower length scale cutoff for this energy.

One can also define an effective mass for the plaquette peripheral boundary. In exchange-coupled magnets, this comes from the tipping of spins caused by wall motion, which can be calculated in the long wavelength regime (1, 37). Here, on a length scale $\sim a_0$, we cannot do this; our long-wavelength theory must therefore write

$$M(R) = M_0 R = 2\pi\sigma_P R, \qquad [5]$$

integrating over a phenomenological mass σ_P per unit length, where $\sigma_P V_w^2 \sim 9.4$ K, and V_w is the Walker velocity.

We thus have an effective action for the plaquette given by

$$S_P^{(1)} = \int \mathrm{d}\tau \left[\frac{1}{2} M(R)\dot{R}^2 - U_0(R)\right] \qquad [6]$$

for a single circular plaquette of radius R. We see that the potential barrier $U_0(R)$ and the action $S_P^{(1)}$ for this single plaquette are of the form characteristic of "bubble nucleation" (here for a two-dimensional bubble), and this nucleation can occur by either thermal activation over the barrier or tunneling through it. Once the plaquette has either surmounted or tunneled through the barrier, so that nucleation has occurred, it will continue to grow.

We emphasize here that the use of the action in this simplified form, where the plaquette is assumed to remain circular, is an approximation, which should work reasonably well for $x = 1$, but for the disordered system $x < 1$ is less secure (see *SI Appendix*, section 2.4 for details). Disorder will have the effect of creating "vacancies" in the lattice periodic potential term of the domain wall energy where magnetic Ho^{3+} ions are replaced by nonmagnetic Y^{3+} ions, since there is no spin to flip, and hence no corresponding energy cost. Furthermore, in the pure crystal, internal dipolar transverse fields exactly cancel out due to crystal symmetry, and so disorder will break this symmetry and allow for transverse fields up to a few kOe (the nearest neighbor sources a transverse field of approximately

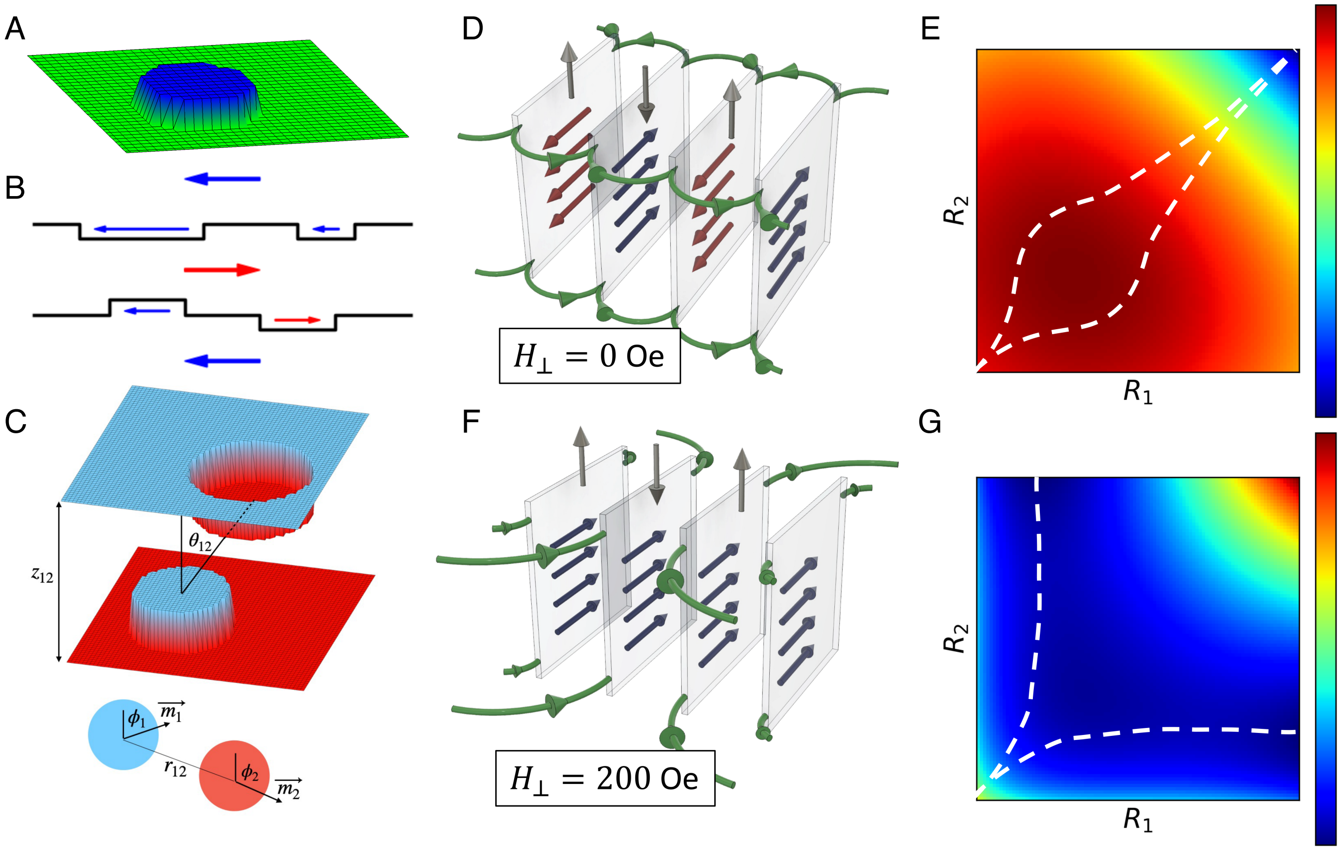

Fig. 4. Domain wall configurations and interaction potentials. (*A*) Schematic of Bloch domain wall with single "plaquette" structure. Grid denotes locations of individual spins. (*B*) Illustration of plaquettes on a pair of adjacent walls. (*C*) Geometry for calculation of the pairwise interaction. The walls are separated by z_{12}, the radial separation between the plaquette centers is ρ_{12} and they are at a polar angle θ_{12} with respect to each other. Magnetization and field directions and tunneling potentials for attractive (*D* and *E*) and repulsive (*F* and *G*) interactions. (*D* and *F*) Vertical gray arrows designate bulk magnetization direction within a domain along the Ising axis, while the red/blue arrows designate the transverse polarizations within a Bloch wall. The green curved arrows illustrate the demagnetization fields. The tunneling potentials (*E* and *G*) are a function of the radii of the two interacting plaquettes, R_1 and R_2, coupled via the dipolar interaction. Tunneling paths that correspond to paths of stationary action will tend to follow paths of minimum potential, and for large R_1, R_2 will be dominated by the quartic interaction term $U^{(4)} \sim R_1^2 R_2^2$. White dashed lines are not the result of numerical calculations, but rather schematics to illustrate the qualitative difference in behavior for the two cases of attractive interaction $U^{(4)} < 0$ (*D* and *E*) and repulsive interaction $U^{(4)} > 0$ (*F* and *G*). (*D*) In zero transverse field, there will be pairs of domain walls with the same transverse polarization as well as domain walls with opposite polarization. We illustrate the case of staggered polarizations of the domain walls at zero transverse field with corresponding attractive interaction $U^{(4)} < 0$ in (*E*) causing R_1 and R_2 to grow together (as indicated by the tunneling paths shown in white). While this schematic shows the staggered case, in zero transverse field, there will not only be adjacent walls of opposite polarization but also adjacent walls of the same polarization as in the case of finite transverse field. (*F*) All walls polarized in the same direction due to the transverse field, with the corresponding repulsive interaction in (*G*), cause plaquettes to grow independently from one another, as indicated by the tunneling paths shown in white.

900 Oe). These will undoubtedly cause some wall roughening and make the actual plaquettes deviate from perfect circles. However, even though analytic calculations including disorder are not plausible, one can still gain considerable qualitative insight from the analysis following the perfectly circular plaquette approximation.

Consider now the case where we have two coplanar flat domain walls lying near to each other (Fig. 4*B*). As seen from side-on, a number of different ways in which plaquettes may nucleate on each wall are shown; these plaquettes will interact with each other. As illustrated in Fig. 4*C*, suppose we have two plaquettes, centered at positions $\vec{r}_1$ and $\vec{r}_2$; they may be either on the same planar wall, or one on each of the two different planar walls. The local fields at the two plaquettes, coming from the combination of external and demagnetization fields, are written $\vec{B}_i = \vec{H}_0 + \vec{H}_{\mathrm{DM}}$. We discuss the size and distribution of the demagnetization field in *SI Appendix*, section 4.

Now we are primarily interested in the case where the plaquettes are small compared to their separation, i.e., when they are in the process of nucleation. We then write the total energy of a pair of plaquettes separated by a distance $r_{12} = |\vec{r}_{12}| = |\vec{r}_1 - \vec{r}_2| \gg R_i$ with $i = 1, 2$, as

$$U_{12} = U_0(\vec{R}_1, \vec{B}_1) + U_0(\vec{R}_2, \vec{B}_2) + \Delta U_{12}, \qquad [7]$$

where $U_0(\vec{R}_i, \vec{B}_i)$ is the single plaquette energy given by Eq. **3**, with local field $\vec{B}_i$ and spin $\vec{\tilde{J}}_i$ per Ho spin in each plaquette, and with the interplaquette interaction given by the dipolar form:

$$\Delta U_{12} = -\frac{\mu_0}{r_{12}^3}(g\mu_B\pi)^2\left[3\frac{(\vec{\tilde{J}}_1\cdot\vec{r}_{12})(\vec{\tilde{J}}_2\cdot\vec{r}_{12})}{r_{12}^2} - \vec{\tilde{J}}_1\cdot\vec{\tilde{J}}_2\right]\frac{R_1^2R_2^2}{a_0^4}. \qquad [8]$$

In addition to the independent tunneling processes of a single plaquette, this interaction term ΔU_{12} gives rise to cotunneling processes involving the dipolar interaction between two plaquettes.

If this interaction term is attractive ($\Delta U_{12} < 0$), then the configuration energy will be minimized by having the radii of both plaquettes (R_1, R_2) growing together. In this picture, attractive interactions between plaquettes on different domain walls can cause cotunneling processes in which nucleation of one plaquette lowers the energy barrier for nucleation of the other. By contrast, if the interaction term is repulsive ($\Delta U_{12} > 0$), then these cotunneling processes are suppressed, and the energetically favored tunneling paths consist of each plaquette growing independently of the other.

The sign of this interaction depends on the relative orientation and polarization of the two plaquettes. If we assume that the plaquettes are opposite each other, and that their polarizations lie along the x-axis, the interaction simplifies to being attractive when the polarizations are aligned and being repulsive when they are antialigned. Hence, the polarizations of domain walls affect the tunneling dynamics by giving rise to cooperative tunneling of pairs of plaquettes on adjacent domain walls when their polarizations are antialigned, in addition to the standard independent tunneling processes of single plaquettes.

While the application of an external longitudinal field simply reduces the height of the tunneling barrier, accelerating plaquette nucleation and domain wall tunneling, application of a sufficiently strong transverse field will act to orient polarizations of all the walls to be parallel to the applied field. While the spatial extent of the measured avalanches is not known, the large number of spins involved in an avalanche ($\sim 10^{15}$ to 10^{16}) guarantees that the wall area will be large. Furthermore, since the Zeeman energy of the wall scales as the number of spins within the wall, the polarizations of these large sections of domain wall will be highly susceptible to even a modest transverse field. Thus, while a small 200 Oe transverse field is much less than the single-ion tunneling field scale ($\sim$20 kOe) (20), or the quantum phase transition (QPT) field scale ($\sim$12 kOe) (6), it is large enough to appreciably polarize most domain walls in the same direction, thereby changing the statistics of the cotunneling processes. We illustrate these two wall configurations in Fig. 4, with the wall polarizations staggered in zero transverse field in panel (*D*), and the configuration with all walls polarized in the same direction in a finite transverse field in panel (*F*).

When the external field is zero, the wall polarizations are random, giving rise to both aligned and antialigned domain wall configurations. Consequently, at zero field, cotunneling processes will be possible due to the attractive interaction between the antialigned domain walls. When a finite transverse field is applied, however, all the walls polarize in the same direction, making all of the interactions between walls repulsive, and consequently suppressing the cotunneling processes. Thus, at zero transverse field both "cooperative events" (due to cotunneling processes) and "independent events" (due to independent tunneling processes) are observed, while at a finite field of 200 Oe only independent events are observed. We plot the corresponding tunneling potentials in Fig. 4 *E* and *G* for the domain wall configurations in panels (*D* and *F*). (*E*) illustrates the attractive interaction due to the staggered polarizations of Bloch walls in zero field; (*G*) illustrates the repulsive interaction due to all wall polarizations being aligned along the external transverse field direction.

We emphasize that, while all domain wall motion is governed primarily through quantum tunneling of small plaquettes, large events consisting of 10^{15} spins are avalanches of many plaquette tunneling events triggering one another—not single coherent macroscopic tunneling events. Once a domain wall is depinned via nucleation of the first plaquette, the form of the avalanche is not dependent on the exact details of plaquette tunneling, but on the structure of the random field pinning resulting from disorder. Even though cotunneling events do not cause entire walls to tunnel together, they can cause simultaneous quantum nucleation of two plaquettes on adjacent walls at once, setting off simultaneous avalanches of pairs of multiple domain walls. They are visible as events with larger area compared to events that were nucleated through independent tunneling.

3. Conclusion

We conclude by summarizing the key results found here. We show that, within the linear regime of a hysteresis loop (dominated by domain wall motion, rather than domain creation/annihilation), the sample dynamics are completely temperature independent up to 95% of T_c, indicating that all domain wall motion is governed by quantum tunneling, rather than thermal activation. Furthermore, there exist two separate classes of Barkhausen events: one class (independent events) that is only weakly affected by the application of a weak transverse field, and another class (cooperative events) of events that have larger area (approximately double) for any given event duration, and whose occurrence is strongly suppressed with a weak external field (almost completely suppressed by 200 Oe).

In addition to independent tunneling of domain wall plaquettes, we propose a second quantum tunneling mechanism where dipolar interactions between neighboring domain walls cause cooperative tunneling that simultaneously nucleates plaquettes on both domain walls, triggering correlated avalanches. These cotunneling processes are the ones that can be suppressed strongly with a modest transverse field—much weaker than any field scale governing either the single-spin tunneling rates or the many-body phase diagram. We see no other explanation for two distinct types of (quantum) avalanche activation mechanisms that is consistent with what we know about the system and with the data.

These experiments involve domain wall motion in a ferromagnet, the prototype for Barkhausen noise measurements. Avalanches, however, occur in a diverse set of physical systems, from photomultiplier tubes, to earthquakes, to plastic deformation of nanostructures, revealing details of a system's energy landscape and reversal dynamics. Our work, venturing into the quantum regime suggests that similar quantum effects should be observable in other systems where long-range interactions between microscopic degrees of freedom can cause correlated activation of macroscopic avalanches, i.e., that one should search for quantum avalanche and quantum Barkhausen effects in a large variety of systems.

4. Materials and Methods

A $4 \times 4 \times 8$ mm^3 tetragonal crystal of $LiHo_{0.4}Y_{0.6}F_4$, with long axis parallel to the Ising axis of the localized Ho^{3+} moments, was mounted in an insulating PEEK coil form to resist torques applied from the external transverse field. A 100-turn inductive pickup coil was wrapped around the center of the sample to measure the time-derivative of the bulk magnetization, and the coil assembly was mounted to the high-purity copper cold-finger of a Helium dilution refrigerator to reach milliKelvin temperature scales. An illustration of the experimental apparatus is included in Fig. 1. Thermal equilibration was aided by heat-sinking the sample to an insulating sapphire plate, which was metalically connected to the Cu cold-finger. External magnetic fields were applied using a superconducting 6T/2T vector magnet, with the longitudinal field ramped between saturation fields $\pm$4 kOe, with a sweep rate $dH_{\|}/dt = 11.1$ Oe/s which we have confirmed to be in the adiabatic limit by comparing ramp rates over a decade down to 1.1 Oe/s . In order to collect suitable statistics of the avalanche events, hundreds of hysteresis loops were taken at a series of temperatures from 90 mK (15% T_c) $\rightarrow$ 580 mK (95% T_c), and transverse fields from 0 Oe $\rightarrow$ 200 Oe. Despite this transverse field scale being an order of magnitude below a known transverse field scale corresponding to quantum speed-up in the same material, no avalanche events were observed above 200 Oe. We illustrate this by plotting the frequency of avalanche events per hysteresis loop as a function of transverse field in Fig. 2*B*.

The quasistatic bulk magnetization of the sample was measured with the use of a GaAs Hall-effect magnetometer (Toshiba THS118) sampling at 1 Hz. We plot individual hysteresis loops at the extreme values of measured temperatures (90 and 580 mK) and transverse fields (0 and 200 Oe) in Fig. 1*C*. There is little variation in the magnetization loops at the different temperatures, and there is no observable difference in sample response from 0 to 200 Oe for any temperature.

In order to measure individual avalanche events, a higher sampling frequency is needed than the 1 Hz sampling of the Hall sensor. Instead of observing avalanches through measurements of the magnetization, the inductive pickup coil converted the time-derivative of the magnetization into a voltage signal, which was further amplified by a high-frequency transformer amplifier (CMR-Direct LTT-h) with a gain of 10 to extend out the frequency response past the 100 kHz attempt frequency of $LiHoF_4$. This voltage signal was further amplified at room temperature by a transistor preamplifier (Stanford Research SR560) with a gain of 5,000 running off of DC battery power, and digitized at a sampling frequency of 1 MHz with an oscilloscope (PicoScope 4262).

Individual avalanche events were extracted from the raw voltage traces using an automated routine that identified events as segments of the data with voltages greater than a threshold calculated to be 3.5σ of the Gaussian-distributed instrumentation noise, after subtracting off a low-frequency (<1 kHz) background. The beginning and ends of each individual event were linearly extrapolated to 0 V that was independent of extrapolation regime. We plot a sample event extraction in Fig. 2*C*.

Data, Materials, and Software Availability. The datasets underlying the figures in this text are available at the CaltechDATA repository, DOI: https://doi.org/10.22002/n3n50-msf83 (31).

ACKNOWLEDGMENTS. We thank R.D. McKenzie for illuminating discussions. The experimental work and the modeling of the data at Caltech were supported by the U.S. Department of Energy Basic Energy Sciences Award No. DE-SC0014866. Theoretical work at UBC was supported by the National Sciences and Engineering Research Council of Canada, No. RGPIN-2019-05582.

1. P. Stamp, E. Chudnovsky, B. Barbara, Quantum tunneling of magnetization in solids. *Int. J. Mod. Phys. B* **6**, 1355–1473 (1992).
2. K. Hong, N. Giordano, Approach to mesoscopic magnetic measurements. *Phys. Rev. B* **51**, 9855–9862 (1995).
3. K. Hong, N. Giordano, Effect of microwaves on domain wall motion in thin Ni wires. *Europhys. Lett.* **36**, 147 (1996).
4. W. Wernsdorfer, R. Clérac, C. Coulon, L. Lecren, H. Miyasaka, Quantum nucleation in a single-chain magnet. *Phys. Rev. Lett.* **95**, 237203 (2005).
5. J. Brooke, T. F. Rosenbaum, G. Aeppli, Tunable quantum tunnelling of magnetic domain walls. *Nature* **413**, 610–613 (2001).
6. D. M. Silevitch, G. Aeppli, T. F. Rosenbaum, Switchable hardening of a ferromagnet at fixed temperature. *Proc. Natl. Acad. Sci. U.S.A.* **107**, 2797–2800 (2010).
7. D. M. Silevitch, J. Xu, C. Tang, K. A. Dahmen, T. F. Rosenbaum, Magnetic domain dynamics in an insulating quantum ferromagnet. *Phys. Rev. B* **100**, 134405 (2019).
8. G. Tatara, H. Fukuyama, Macroscopic quantum tunneling of a domain wall in a ferromagnetic metal. *J. Phys. Soc. Japan* **63**, 2538–2562 (1994).
9. G. Tatara, H. Fukuyama, Macroscopic quantum tunneling of a domain wall in a ferromagnetic metal. *Phys. Rev. Lett.* **72**, 772–775 (1994).
10. P. C. E. Stamp, Quantum dynamics and tunneling of domain walls in ferromagnetic insulators. *Phys. Rev. Lett.* **66**, 2802–2805 (1991).
11. M. Dubé, P. C. E. Stamp, Effects of phonons and nuclear spins on the tunneling of a domain wall. *J. Low Temp. Phys.* **110**, 779–840 (1998).
12. S. Takagi, G. Tatara, Macroscopic quantum coherence of chirality of a domain wall in ferromagnets. *Phys. Rev. B* **54**, 9920–9923 (1996).
13. E. G. Galkina, B. A. Ivanov, S. Savel'ev, F. Nori, Chirality tunneling and quantum dynamics for domain walls in mesoscopic ferromagnets. *Phys. Rev. B* **77**, 134425 (2008).
14. H. Barkhausen, *Phys. Z.* **20** (1919).
15. K. Dahmen, J. P. Sethna, Hysteresis, avalanches, and disorder-induced critical scaling: A renormalization-group approach. *Phys. Rev. B* **53**, 14872–14905 (1996).
16. B. Alessandro, C. Beatrice, G. Bertotti, A. Montorsi, Domain-wall dynamics and Barkhausen effect in metallic ferromagnetic materials. I. Theory. *J. Appl. Phys.* **68**, 2901–2907 (1990).
17. G. Durin, S. Zapperi, *The Barkhausen Effect* (Elsevier, 2006), vol. 2, pp. 181–267.
18. F. Bohn *et al*., Playing with universality classes of Barkhausen avalanches. *Sci. Rep.* **8**, 11294 (2018).
19. I. P. de Sousa *et al*., Waiting-time statistics in magnetic systems. *Sci. Rep.* **10**, 9692 (2020).
20. M. Schechter, P. C. E. Stamp, Significance of the hyperfine interactions in the phase diagram of $LiHo_xY_{1-x}F_4$. *Phys. Rev. Lett.* **95**, 267208 (2005).
21. M. Schechter, P. C. E. Stamp, Derivation of the low-*T* phase diagram of $LiHo_xY_{1-x}F_4$: A dipolar quantum Ising magnet. *Phys. Rev. B* **78**, 054438 (2008).
22. M. Schechter, N. Laflorencie, Quantum spin glass and the dipolar interaction. *Phys. Rev. Lett.* **97**, 137204 (2006).
23. T. Egami, Theory of intrinsic magnetic after-effect. I. Thermally activated process. *Phys. Status Solidi A* **19**, 747–758 (1973).
24. T. Egami, Theory of intrinsic magneitc after-effect. II. Tunnelling process and comparison with experiments. *Phys. Status Solidi A* **20**, 157–165 (1973).
25. P. Jorba, SHPM imaging of $LiHoF_4$ at ultra low temperatures, Master's thesis (Ecole Polytechnique Federale de Lausanne, Lausanne, Switzerland, 2014).
26. P. Meyer, J. Pommier, J. Ferre, Magnetooptic observation of domains at low temperature in the transparent ferromagnet $LiHoF_4$. *Electro-Opt. Magneto-Opt. Mater. Appl.* **1126**, 93–98 (1989).
27. A. Herpin, *Théorie du Magnétisme, Bibliothèque des Sciences et Techniques Nucléaires* (Institut national des sciences et techniques nuclèaires, PUF, Saclay, Paris, France, 1968).
28. T. Dollberg, J. C. Andresen, M. Schechter, Effect of intrinsic quantum fluctuations on the phase diagram of anisotropic dipolar magnets. *Phys. Rev. B* **105**, L180413 (2022).
29. O. Perković, K. Dahmen, J. P. Sethna, Avalanches, Barkhausen noise, and plain old criticality. *Phys. Rev. Lett.* **75**, 4528–4531 (1995).
30. S. Zapperi, P. Cizeau, G. Durin, H. E. Stanley, Dynamics of a ferromagnetic domain wall: Avalanches, depinning transition, and the Barkhausen effect. *Phys. Rev. B* **58**, 6353–6366 (1998).
31. C. Simon, Data from "Barkhausen Noise Dataset $4\times4\times8$mm LiHo_0.4Y_0.6F_4." CaltechDATA. https://doi.org/10.22002/n3n50-msf83. Deposited 25 January 2024.
32. S. Zapperi, C. Castellano, F. Colaiori, G. Durin, Signature of effective mass in crackling-noise asymmetry. *Nat. Phys.* **1**, 46–49 (2005).
33. S. Papanikolaou *et al*., Universality beyond power laws and the average avalanche shape. *Nat. Phys.* **7**, 316–320 (2011).
34. G. Durin *et al*., Quantitative scaling of magnetic avalanches. *Phys. Rev. Lett.* **117**, 087201 (2016).
35. G. Mennenga, L. J. de Jongh, W. J. Huiskamp, Field dependent specific heat study of the dipolar Ising ferromagnet $LiHoF_4$. *J. Magnet. Magnet. Mater.* **44**, 59–76 (1984).
36. G. I. Mias, S. M. Girvin, Absence of domain wall roughening in a transverse-field Ising model with long-range interactions. *Phys. Rev. B* **72**, 064411 (2005).
37. T. Nakamura, Y. Kanno, S. Takagi, Single-collective-degree-of-freedom models of macroscopic quantum nucleation. *Phys. Rev. B* **51**, 8446–8456 (1995).